Available online at www.sciencedirect.com
SCIENCE DIRECT®
Journal of volcanology and geothermal research
ELSEVIER
Journal of Volcanology and Geothermal Research 153 (2006) 51–63
www.elsevier.com/locate/jvolgeores

Waveform classification of volcanic low-frequency earthquake swarms and its implication at Soufrière Hills Volcano, Montserrat

David N. Green *, Jürgen Neuberg

School of Earth Sciences, University of Leeds, Leeds, LS2 9JT, UK

Received 6 May 2004; received in revised form 23 January 2005; accepted 17 August 2005
Available online 6 January 2006

Abstract

Low-frequency volcanic earthquakes are indicators of magma transport and activity within shallow conduit systems. At a number of volcanoes, these events exhibit a high degree of waveform similarity providing a criterion for classification. Using cross-correlation techniques to quantify the degree of similarity, we develop a method to sort events into families containing comparable waveforms. Events within a family have been triggered within one small source volume from which the seismic wave has then travelled along an identical path to the receiver. This method was applied to a series of 16 low-frequency earthquake swarms, well correlated with cyclic deformation recorded by tiltmeters, at Soufrière Hills Volcano, Montserrat, in June 1997. Nine waveform groups were identified containing more than 45 events each. The families are repeated across swarms with only small changes in waveform, indicating that the seismic source location is stable with time. The low-frequency seismic swarms begin prior to the point at which inflation starts to decelerate, suggesting that the seismicity indicates or even initiates a depressurisation process. A major dome collapse occurred within the time window considered, removing the top 100 m of the dome. This event caused activity within some families to pause for several cycles before reappearing. This shows that the collapse did not permanently disrupt the source mechanism or the path of the seismic waves.
© 2005 Elsevier B.V. All rights reserved.

Keywords: volcano; waveform; classification; cross-correlation; low-frequency earthquakes; swarms; Montserrat

1. Introduction

Low-frequency earthquakes in volcanic environments have been used to infer and assess the characteristics of shallow conduit systems (Gil Cruz and Chouet, 1997; Neuberg, 2000). These events often occur in highly ordered swarms with many hundreds of earthquakes triggered within a few hours. Therefore, for detailed analysis of the activity, events must be classified into groups that reflect a certain physical meaning.

Classification schemes often choose to subdivide series of signals according to frequency content (Power et al., 1994; Miller et al., 1998), which often divides these events into two groups dependent upon how much of the signal power is concentrated at relatively high (>5 Hz) frequencies. High frequencies are interpreted as being the result of brittle fracture whereas low-frequency coda, with characteristic peaked spectra between 0.2 and 5 Hz, are thought to be associated with the resonance of a crack or a conduit section (Chouet, 1988; Neuberg et al., 2000).

In contrast, waveforms provide detailed information on the path that the seismic wave has taken from the source to the seismometer, including all interfaces

* Corresponding author. Fax: +44 113 343 5259.
E-mail address: dng@earth.leeds.ac.uk (D.N. Green).

0377-0273/$ - see front matter © 2005 Elsevier B.V. All rights reserved.
doi:10.1016/j.jvolgeores.2005.08.003

along which the wave has travelled, been reflected at or transmitted through. A classification scheme based on the similarity of waveforms uses this information to group events according to the source location and the parameters of any structure in which the seismic waves have been trapped.

Stephens and Chouet (2001) and Umakoshi et al. (2003) have grouped events into families of earthquakes with similar waveforms using cross-correlation techniques to quantify event similarity. Stephens and Chouet (2001) found the majority of events for a swarm at Mt. Redoubt, Alaska, belonged to one family whose waveform evolved slowly over the 18-h swarm. Similar evolving waveforms were also observed at Mt. Unzen, Japan (Umakoshi et al., 2003), with over 70 families identified containing more than 100 similar earthquakes each over a time period of 2 months.

This paper presents a waveform analysis for a series of low-frequency earthquake swarms occurring during June 1997 at Soufrière Hills Volcano, Montserrat, West Indies. This andesitic volcano has been active since 1995 and has undergone a series of dome building episodes with subsequent collapse, punctuated by periods of Vulcanian explosions. Low-frequency seismicity has been common throughout and White et al. (1998) remarked on the similarity of low-frequency earthquake waveforms in the early stages of the eruption.

The period of June 1997 is of particular interest due to the cyclic deformation observed on tiltmeters located close to the active dome (Voight et al., 1998). From mid-May until June 22nd, when the emplacement of a subhorizontal shear lobe had promoted dome growth towards the north, few low-frequency earthquakes were recorded (<20 events/day triggered the Montserrat Volcano Observatory auto-detection software). Throughout this period, the extrusion rate was estimated as approximately 4–5 $m^3\ s^{-1}$(Watts et al., 2002). On June 22nd, a rapid increase of low-frequency seismicity was observed, with over 300 triggered events/day recorded within periodic swarms. These swarms coincided with cycles of dome inflation and deflation, which had a periodicity of approximately 10 h (Fig. 1). The high-amplitude shallow pressurisation cycles continued for the next 2 weeks, but were punctuated by a dome collapse at approximately 12:45 on the 25th June, which removed ca. 6.4×10^6 m^3 of material from the top of the edifice (Watts et al., 2002). Periodic deformation and seismic swarms continued after the collapse with a decreased periodicity of approximately 8 h and an increased amplitude.

Voight et al. (1998) remarked on how the seismicity increased in intensity when the tilt cycles reached a peak value, and Voight et al. (1999) suggested hybrid seismicity was initiated once a threshold pressure was exceeded. In contrast, Neuberg et al. (2006-this issue) demonstrated that the onset of seismicity is well correlated with the time at which the 'rate of inflation' reaches a maximum, i.e. the point at which the inflation starts to slow, not a threshold value.

These observations provide motivation for the work described in the following sections. Do families of events with similar waveforms exist? Do they indicate that the position of seismicity generation migrates with time, or are the source locations extremely stable? The strong correlation between deformation and low-frequency seismicity suggests there is a physical mechanism, which links the cyclicity observed in both parameters. Can waveform classification help to elucidate this relationship?

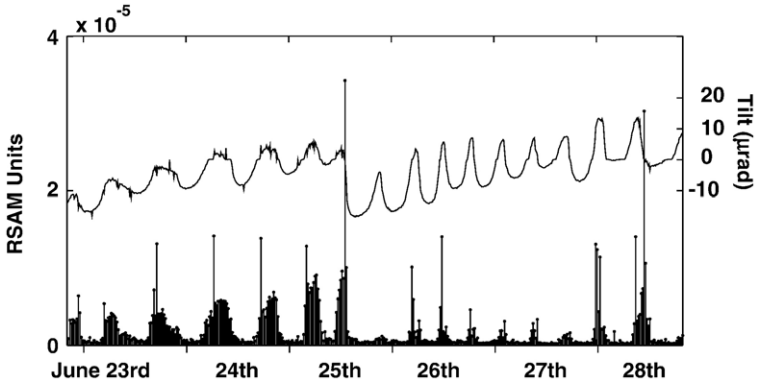

Fig. 1. The deformation cycles and associated seismic activity from June 23rd to June 28th, 1997. The relative seismic amplitude (RSAM) is calculated for 20-min windows using the seismic record at station MBGA, filtered between 0.5 and 5 Hz in order to reduce the influence of high frequency rockfall signals. The dome collapse occurs at approximately 12:45 on June 25th, notable for the high RSAM signal associated with the large pyroclastic flows.

A method similar to that of Stephens and Chouet (2001) for classifying low-frequency events by exploiting the high linear correlation between waveforms is developed in Section 2. The results of the classification and the temporal structure of the waveform families are detailed in Section 3. Implications of these results for the source of low-frequency events and the link to shallow deformation are discussed in Section 4.

2. Methodology

2.1. Classification input

The input to the classification are continuous, broadband, vertical-component seismograms. For the analysis from Soufrière Hills Volcano, the data were recorded by the Montserrat Volcano Observatory staff on a Guralp 40T broadband seismometer, MBGA (Fig. 2), with a sampling frequency of 75 Hz. The instrument response and digitiser gain were removed to give calibrated velocity seismograms. At approximately 1 km from the active dome, MBGA is the closest station to the volcano and as such provides the best signal to noise ratio. For completeness, the analysis was undertaken for other stations on the Montserrat network, with no significant differences being observed in the results except a reduction in event detection.

The input event catalogue for the classification procedure was selected manually in order to identify the majority of events, regardless of waveform similarity. The traces were filtered with a zero-phase band-pass Butterworth two-pole filter. A low-frequency cutoff of 0.5 Hz was chosen to reduce the influence of oceanic microseisms and a high-frequency cutoff of 5 Hz was selected to allow for an effective and efficient event selection. To test that the classification is robust, regardless of the high-frequency filter characteristics, the procedure was conducted with a series of cutoff levels ranging between 5 Hz and the Nyquist frequency. This produced no significant changes in the classification, with 90% of events remaining within the same groupings, due to the majority of the signal power concentrated between 0.2 and 5 Hz.

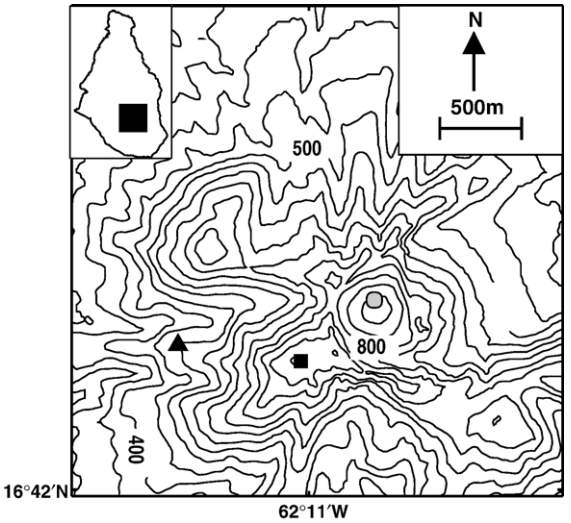

Fig. 2. Map of Soufrière Hills Volcano summit. The triangle gives the position of the three-component broadband seismometer, MBGA. The square gives the position of the tiltmeter, CP2, and the gray circle shows the approximate position of the active vent. Contour heights are given in metres and increment at 50-m levels. The inset shows the location of the map in relation to the island of Montserrat.

The similarity between events is quantified by using the cross-correlation function,

$$r_{xy}(i, i-l) = \frac{\sum_{i=1}^{n}(x_i-\bar{x})(y_{i-l}-\bar{y})}{\sqrt{\sum_{i=1}^{n}(x_i-\bar{x})^2}\sqrt{\sum_{i=1}^{n}(y_{i-l}-\bar{y})^2}} \quad (1)$$

where x_i is the ith sample of the signal x, y_{i-l} is the $(i-l)$th sample of the signal y and the overbar represents the mean value of the signal. The index l is the lag between the two signals; changing this parameter varies the relative position of signal x with respect to signal y. It is noted that the correlation function, r_{xy}, only measures the relative similarity of the waveform shape and not the amplitude of the events, thus giving a measure of the path which the seismic energy takes, not the magnitude of the trigger. For the cross-correlation, an empirically selected window length of 8 s was chosen (Fig. 3), so as to utilise the longest record possible without interference from adjacent events within the most intense swarm series. With the event windows isolated from the seismogram, each event was cross-correlated with every other event. A maximum correlation coefficient matrix, **m**, of size $n \times n$ for a swarm containing n events was constructed, with element m_{xy} representing the maximum of the correlation function between the two events x and y.

2.2. Choice of correlation threshold

The classification clusters earthquakes into groups with similar waveforms. This requires a threshold correlation coefficient, ψ, to be chosen that separates events within a particular waveform family from all others. The choice of this value is a trade-off between classification accuracy and event detection. If ψ is too

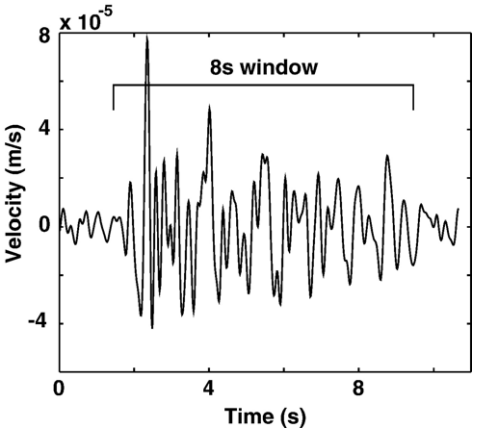

Fig. 3. An example of a typical low-frequency event recorded at station MBGA on Montserrat. The recording is corrected for the instrument response and the digitiser gain. The 8-s window refers to the portion of the signal used within the cross-correlation analysis.

low, waveforms which have slightly different structure can be classified into one group; if ψ is too high, poor signal-to-noise ratios lead to many family members not being classified at all. Table 1 shows the results of changing the coefficient, ψ, for 600 synthetic events of 600 samples length with added random noise of the same spectral bandwidth as the signals. The noise amplitudes generated were normally distributed, so as to produce a mean signal-to-noise ratio of 7 dB with a standard deviation of 3 dB. These tests show that for $\psi = 0.75$ events with signal-to-noise ratios less than 5 dB are regularly rejected, in good agreement with the results of Stephens and Chouet (2001) (their Fig. 7) who used $\psi = 0.68$ with a 10-s correlation window. Another implication of these tests is that small events, whose signal-to-noise ratios are necessarily lower, have smaller correlation coefficients with other events although the signal may be identical.

Table 1
The percentages of each waveform family correctly classified while testing the choice of detection threshold parameter, ψ

Family	% Events classified correctly			
Threshold (ψ)	Family X	Family Y	Family Z	Total
0.80	66	20	59	48
0.75	82	36	74	64
0.70	90	50	87	76
0.65	97	66	93	85
0.60	Families X and Z merge			

The three families, X, Y and Z, contain 200 events each, with the signal to noise levels normally distributed with a mean of 7 dB and a standard deviation of 3 dB. The maximum cross-correlation between the three waveforms without noise added are $r_{xy} = 0.45$, $r_{xz} = 0.61$ and $r_{yz} = 0.50$.

With the above considerations taken into account, a value of $\psi = 0.70$ was chosen for all subsequent analysis. This allows the majority of events with signal-to-noise ratios ≥ 5 dB to be detected; yet, it is above the correlation levels where correct classification may start to break down. Further justification for this level is given in Fig. 4, which shows the distribution of correlation coefficients for a half hour seismogram cross-correlated with a particular seismic wavelet known to be present within the data. It is seen that the majority of coefficients form a normal distribution as expected for the random correlations between wavelet and noise. However, the upper tail of the distribution clearly shows the presence of well-correlated events and the threshold value of $\psi = 0.70$ is well above the upper noise limit.

2.3. Classification procedure

To sort the matrix **m** into families, the event with the most correlation values above the threshold value, ψ, was isolated and chosen as a master event for the first waveform family. All the events well correlated with it ($r \geq \psi$) were removed from the matrix as one group. This left a remainder matrix to which the same process was applied until the entire matrix is classified into distinct groups.

The above method produces a thorough classification; however, the use of a master event, although correlated with more events than any other, may produce a selection bias. To reduce this bias, an average family waveform was found by stacking all events within a group. This stack was then cross-correlated with the original seismic record and all events with a

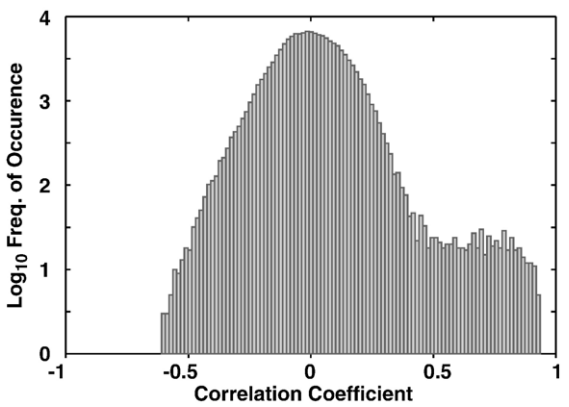

Fig. 4. The distribution of cross-correlation coefficients for a 30-min data series from the MBGA station when cross-correlated with a waveform family stack known to be present within it. The distribution is presented with a logarithmic scale in order to highlight the presence of events where the cross-correlation values are above those which are expected from a continuation of the normally distributed curve.

correlation greater than the threshold, ψ, were grouped into a waveform family. This automatic identification has the advantage of detecting any events belonging to the groups that may have been missed in the manual picking stage. However, this introduces an ambiguity. Using only the manually isolated events produced groups that were independent but by employing an autopicking routine with several stacked waveforms over the same trace, there is no requirement for all families to be mutually exclusive. This phenomenon was accounted for and any events that bridge different groups were identified.

3. Results

Continuous data for the 6-day period from the 23rd to the 28th June 1997 was analysed, with the 48 h of the 25th and 26th June used for the initial cross-correlation classification. The seismic results were then compared to the deformation recorded at a tiltmeter positioned at Chances Peak, approximately 650 m from the active vent (Fig. 2).

3.1. Family detection

Within the 6-day analysis period, 9 waveform families containing more than 45 events each were observed (Table 2). Of these, three contained events, which could be classified into more than one group, and the remaining six had no overlap with other families (Table 3). The three overlapping groups are named A1 to A3, respectively, and only events falling exclusively into these classifications were included here. Another category was produced for events falling into two or more of the A1 to A3 families, called the A composite (ACP) group (Table 2). The remaining six families are referred to as B to G. Examples of waveforms for families A1 and B are given in Fig. 5. The average normalised amplitude spectra of the families highlight the difference between the families (Fig. 6).

Table 2
Sizes of the waveform families found for the 23rd to the 28th June inclusive

Family	No. of events	Family	No. of events
A1	973	C	139
A2	292	D	75
A3	165	E	116
ACP	764	F	47
B	306	G	53

The family labelled 'ACP' includes all events, which fall into more than one of the A1 to A3 categories.

Table 3
The cross-correlation coefficients between the average family waveforms used to identify members of the waveform families

A1	A2	A3	B	C	D	E	F	G	
1	**0.69**	**0.66**	0.41	0.36	0.47	0.38	0.50	0.32	A1
	1	**0.64**	0.40	0.37	0.53	0.37	0.46	0.25	A2
		1	0.32	0.39	0.17	0.31	**0.66**	0.35	A3
			1	0.38	0.60	0.39	0.21	0.29	B
				1	0.45	0.31	0.44	0.56	C
					1	0.35	0.22	0.30	D
						1	0.36	0.43	E
							1	0.35	F
								1	G

Any correlation above 0.6 is highlighted to indicate that these families are closely related. Family names are given above/adjacent to each column/row.

Groups A1 to A3 have consistent spectral peaks with some members having higher proportions of low-frequency (1–3 Hz) power than others. The remaining families have no consistent spectral peaks.

Fig. 7 demonstrates that each family has a particular amplitude distribution, with the families A1 to A3 having mean peak-to-peak values higher than those of families C through to G. Family B has a mean comparable to the A families but is notable in that it has maximum values more than double those for any other family. No consistent temporal evolution of the amplitudes are observed, with all swarms having mean family amplitudes which lie within one standard deviation of the total distributions.

To ensure the classification is robust, the events were reclassified using a range of threshold coefficients as in Section 2.2. The results are given in Table 4, showing that for six of the nine families (B to G) the threshold has no effect on the classification except to subdivide two families when $\psi = 0.8$. Families A1, A2 and A3, as expected from their high cross-correlation coefficients, are shown to be subsets of a larger family at $\psi = 0.6$. The choice of $\psi = 0.7$ is justified, as it provides a balance between detail of classification and event detection.

When classified using $\psi = 0.7$, the large families account for 51% of the picked data, showing that not all low-frequency seismic events belong to waveform families. At $\psi = 0.6$, this figure increase to 60%.

3.2. Seismicity and tilt

A family is defined as being active between the onset time of the first event in a particular swarm, such that no events in the family occur in the previous 2 h, and the onset time of the last event, such that no events in the family occur in the subsequent 2 h. Within

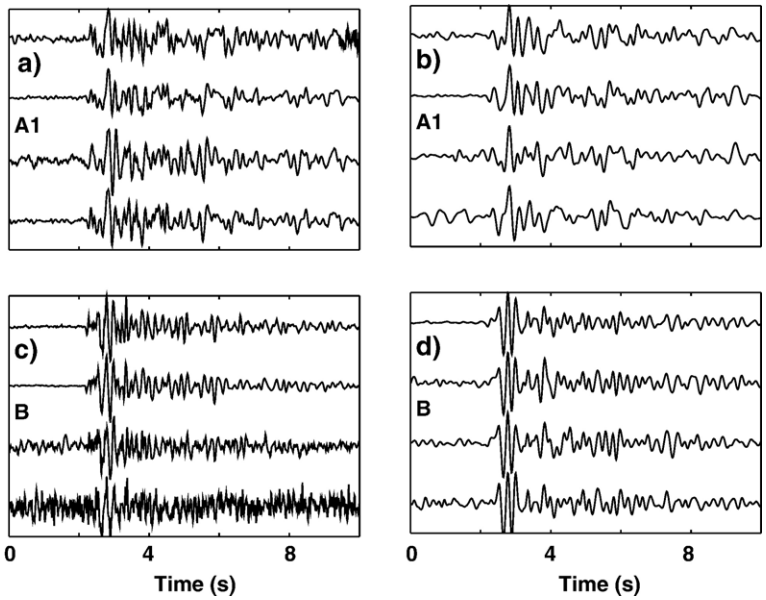

Fig. 5. Examples of the event waveforms for families A1 (a and b) and B (c and d). The left-hand panels give the unfiltered traces, normalised to maximum height. The difference in relative noise level is predominantly an effect of the different event amplitudes. The right-hand panels show the same traces filtered using a Butterworth two-pole filter, with frequency cutoffs at 0.5 Hz and 5 Hz.

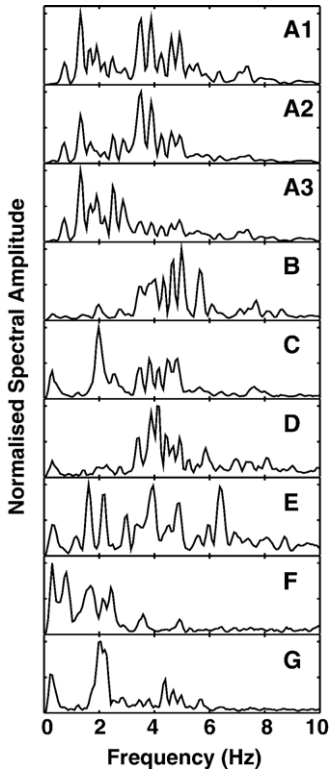

Fig. 6. The stacked normalised amplitude spectra of the nine waveform families. Note that A1, A2 and A3 have consistent spectral peaks, whereas the other six families exhibit marked spectral differences.

any particular swarm, up to seven of the nine families can be active. The initiation and cessation of each family within a particular swarm is staggered, with some waveform sources being triggered earlier than others (Fig. 8). However, when compared to the tilt cycles, the initiation of the first low-frequency earthquake family within a swarm is always observed to lead the maximum of the first time derivative of tilt with a

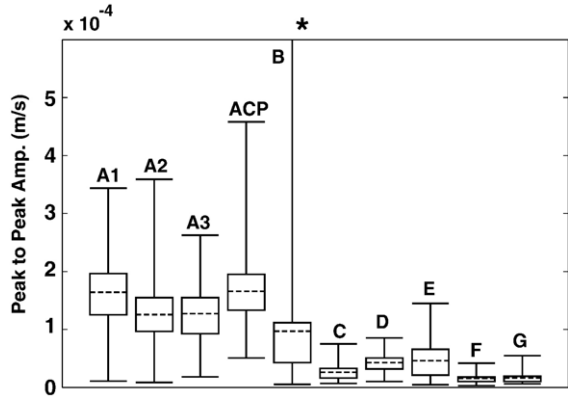

Fig. 7. The peak-to-peak amplitude distributions of the classified events from June 23rd to June 28th. The whisker plots have a base line representing the minimum amplitude recorded for the family and a box enclosing all events between the 25% and 75% quartiles. The dashed line is the distribution mean and the top line is the maximum amplitude recorded. The star above family B indicates that four events are above the plot limit, with the maximum amplitude recorded for this family being 1.9×10^{-3} m s^{-1}.

Table 4
The effect of changing the classification scheme correlation threshold, ψ

Threshold	Family Classification / No. of Events								
0.6	I		II	III	IV	V	VI	VII	VIII
	1035		64	204	148	76	34	38	35
0.7	A1	A2	A3	B	C	D	E	F	G
	876	97	48	133	102	48	27	20	20
0.8	13 families			1 family	4 families	2 families	1 family	1 family	1 family
	826			76	66	33	14	8	8

The table lists the number of events per family in the classification of 2712 earthquakes from June 25th/June 26th for families with 20 members or more at $\psi = 0.7$. As the threshold coefficient is increased, the classification becomes more detailed with families classified at lower threshold levels being subdivided into smaller groups. Less events in total are classified into families when using higher threshold coefficients as earthquakes with low signal to noise ratios are rejected. For example, family VI at $\psi = 0.6$ contains the same events as family E at $\psi = 0.7$ and one family at $\psi = 0.8$, whereas families I and II at $\psi = 0.6$ subdivide into the three A families at $\psi = 0.7$ and 13 families at $\psi = 0.8$.

mean value of 0.95 h (and a S.D. = 0.75 h). In addition, the low-frequency families active at the end of the swarm stop within an hour of the time when the minima in the first derivative of tilt is reached (the families cease, on average, 0.12 ± 0.94 h before the inflection point).

Although there are periods of quiescence of 3 to 7 h between the different swarms, the waveform families are persistent across swarms (Fig. 8), suggesting that sources at the same locations are being activated repeatedly. Also, the order of initiation across swarms remains constant for many families. For example, the four swarms after the dome collapse on the 25th June proceed with family F appearing first, then B, D and E grouped closely in the centre, and families C and G completing the sequence (Figs. 8 and 9).

The rate of overall low-frequency earthquake generation within the swarms reaches a maximum coincident with the maximum of tilt (Voight et al., 1999). This pattern is also observed if only the events associated with the waveform families are considered, with the rate of activity after the maximum declining slowly until the swarm stops. Between swarms, there are low levels of low-frequency seismicity (<20 events/h); however, none of these events belong to the classified families, which occur only in the well-organised swarm structures.

3.3. Time evolution of waveforms

Both Stephens and Chouet (2001) and Umakoshi et al. (2003) observe the waveform within families evolving with time on Redoubt Volcano and Mt. Unzen, respectively. In these studies, the source is active continuously over the analysis period although the activity lasted 18 h in Alaska compared to the swarms in Japan, which lasted up to 20 days.

On Montserrat, only minor evolution of the waveform is observed when studying the development of the correlation coefficient across the swarms, with <0.15 change in the coefficient over 6 days. Fig. 10 demon-

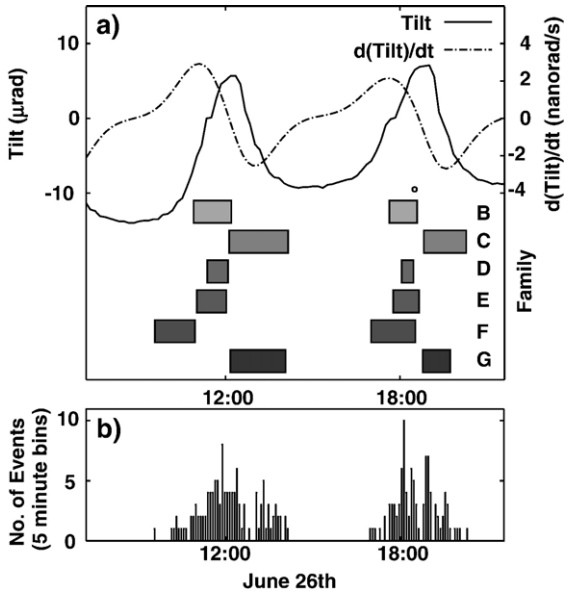

Fig. 8. (a) An example of the occurrence of waveform families in relation to the tilt cycles and the derivative of tilt from June 26th, 1997. The tilt derivative is obtained from a low-pass (characteristic period of 1.5 h) zero-phase filtered tilt record. The oblongs represent the families, with different shades distinguishing between the different waveform groups B to G. The start of the oblong is positioned where the first event of that family occurs in that swarm and the end coincides with the last event. (b) shows the number of events, belonging to all the classified waveform families, for consecutive 5-min bins.

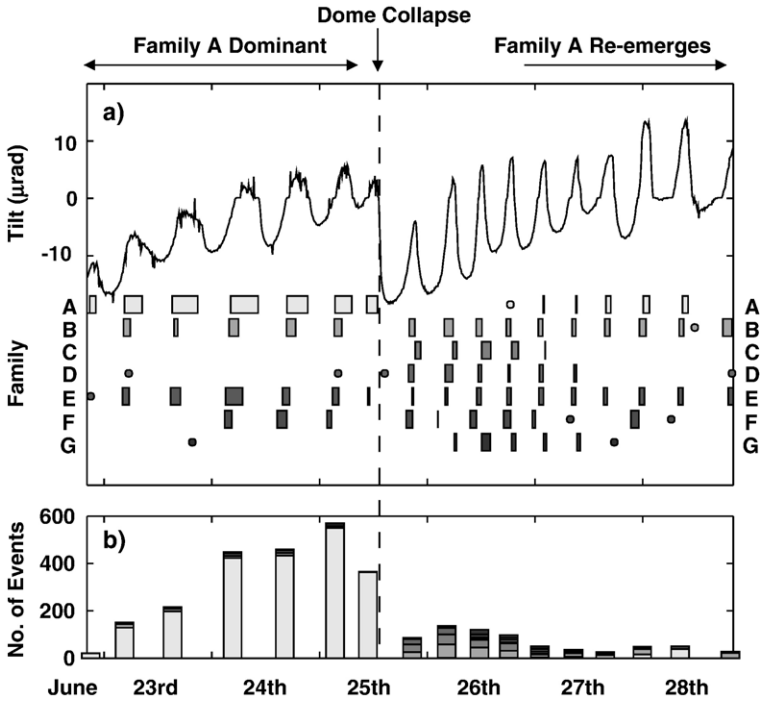

Fig. 9. (a) The occurrence of the waveform families in relation to the tilt between the 23rd June and the 28th June inclusive. The oblongs represent the families, with different shades distinguishing between the different waveform groups A to G (family A is the combined events of families A1, A2, A3 and ACP from Table 2). The start of the oblong is positioned where the first event of the family occurs in each swarm and the end coincides with the last event. The dome collapse occurred at approximately 12:45 on the 25th June as indicated by the dashed line. (b) Histograms showing the number of events per swarm for each family with the same shading as in (a). Note that family A is dominant before the dome collapse, whereas swarms immediately after the event contain high numbers of families B to E.

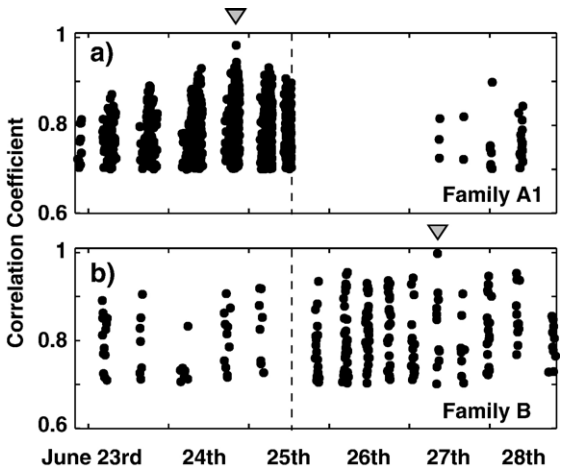

Fig. 10. The evolution of waveforms over time for families A1 and B. For this analysis, the event from each family with the highest signal to noise ratio was chosen as a reference event, the position of which is indicated by a triangle above the plot. All events having a correlation coefficient >0.7 with the reference are plotted against time; (a) represents family A1 and (b) family B. The dome collapse occurs at approximately 12:45 on the 25th June as indicated by the dashed line.

strates the behaviour for the waveform families A1 and B. Both families exhibit a decrease in the maximum correlation coefficient for each swarm successively further separated from the reference event. This pattern is exaggerated by the small numbers of events in distant swarms. Fig. 11 shows the coefficient evolution with event number. This clearly indicates that there is no pattern of evolution within each swarm. All other families show this form of behaviour.

3.4. Influence of the dome collapse

The major dome collapse on the 25th June separates two distinct patterns of deformation, with the periodicity of the cycles decreasing from 11 to 8 h after the event and the amplitude increasing from a mean value of 10 to 16 radians (Fig. 9). A marked change in seismicity is also observed with the number of low-frequency events within families decreasing from >550 events in the last full swarm before the collapse to <100 in the swarm immediately following the event. There is a corresponding drop in the maximum seismicity rate from 7 events/min to 2 events/min.

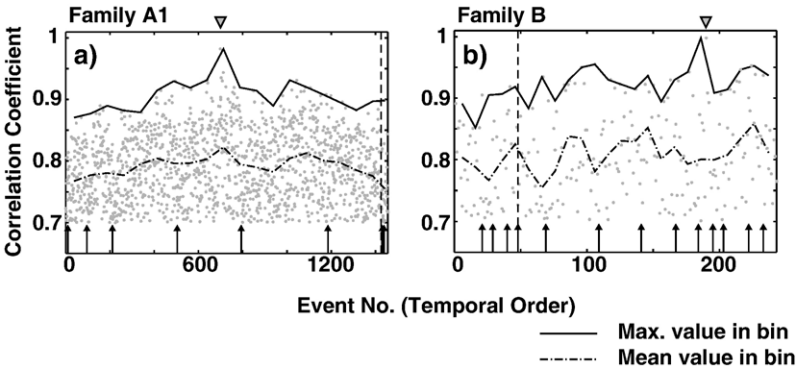

Fig. 11. The evolution of two family waveforms with respect to the event number. These datasets contain all events for the 6 days, which are well-correlated (correlation coefficient >0.7) with a reference event shown by the triangles above the plot. (a) illustrates the evolution of family A1 and (b) illustrates the evolution of family B for comparison with Fig. 10. The vertical dotted lines in both plots represents the position of the dome collapse and the arrows at the base of the plot represent the events which end each swarm. Mean and max values for binned data are also plotted; bins consist of 100 consecutive events for (a) and 10 events for (b).

The predominant waveform groups before the collapse were the A families, yet they are completely absent from the three tilt cycles, a period of 28 h, immediately following the destruction of the dome. These families start to reappear late on the 26th June. There is no correlation between the absolute value of tilt and the appearance of this set of families, as they would reappear by the second swarm after the collapse.

The remaining six families all undergo a considerable increase of activity in the swarms immediately following the dome collapse, except E which shows a marked decrease in activity. Families C and G are short lived, only being active for the first seven swarms following the dome failure.

4. Implications and discussion

The presence of waveform families implies a stable source location for the low-frequency earthquakes. Using the quarter-wavelength hypothesis (Geller and Mueller, 1980), with a P-wave velocity in the source region of 3000 m s^{-1} and a dominant signal frequency of 4 Hz, a conservative estimate of the source volume for each family has a radius of approximately 200 m. However, in environs where seismic activity is initiated by a strong P-phase, relative relocation has shown events within earthquake families may be separated by <100 m (Fremont and Malone, 1987). Relative relocation for low-frequency earthquakes upon Montserrat has proven extremely difficult due to low signal-to-noise ratios but improved absolute locations utilising the waveform groups have been obtained (Neuberg et al., 2006). This analysis places the source of the seismicity within a narrow band at a depth approximately 1500 m below the active dome.

Our analysis shows that these source locations can remain stable for at least 6 days, during periods of shallow deformation and vigorous magma extrusion, and yet the repose time between similar events can be as short as 8 s requiring a source mechanism which is easily recharged. This structure is comparable to that at Mt. Unzen where families are stable for long periods yet are highly active throughout (Umakoshi et al., 2002).

4.1. Characteristic family properties

Models of low-frequency earthquake generation indicate that the event coda is radiated by energy trapped at the interface of a resonating body (Chouet, 1988; Neuberg et al., 2000). The geometrical and material properties of such a structure determine the dominant frequencies of the resulting seismic wave-field. As 8-s windows are used for the cross-correlation analysis, the event coda provides the majority of the information used in the classification. Therefore, the results reflect not only the source location but also the possible structures in which resonating interface waves have been trapped.

The presence of a series of independent families which have different characteristic spectral peaks suggests that a number of resonating bodies are active on Monserrat at any one time. One resonator, corresponding to the ‘A’ families, is more active than the others. The classification of this group of events into separate waveform families (A1, A2, etc.) may be caused by the trigger of the event occurring at different locations throughout the body, preferentially exciting different resonance modes (Chouet, 1988).

The different distributions of event amplitudes indicate that the triggers of seismic energy are of different

sizes. This assumes that all events come from approximately the same region of the conduit, as indicated by Rowe et al. (2004) and Neuberg et al. (2006-this issue), such that the event amplitude is indicative of the source size and not a path effect. The more active 'A' families have larger amplitudes suggesting that more energy per event is released in the most active region.

The lack of waveform evolution through time in this study differs from observations at other volcanoes (e.g. Umakoshi et al., 2002). There appears to be little change over individual swarms or the 6-day series as a whole. This implies the source location is extremely stable, even in this period of active deformation. Indeed, if the seismic energy was trapped within a conduit section undergoing significant pressure changes during a tilt cycle, the seismic velocities would change due to variations in the volume fraction of exsolved gas (Sturton and Neuberg, 2003). This would modify the waveforms, which is not observed either because the changes are too small to be measured or the resonating structure is not subjected to significant pressure fluctuations. The possibility that the lack of evolution is due to the seismic source being below the gas nucleation depth, so that pressure variations have little effect on the seismic velocity, is unlikely at Soufrière Hills Volcano where gas is thought to begin exsolution at a magma chamber depth of 5000 m (Barclay et al., 1998).

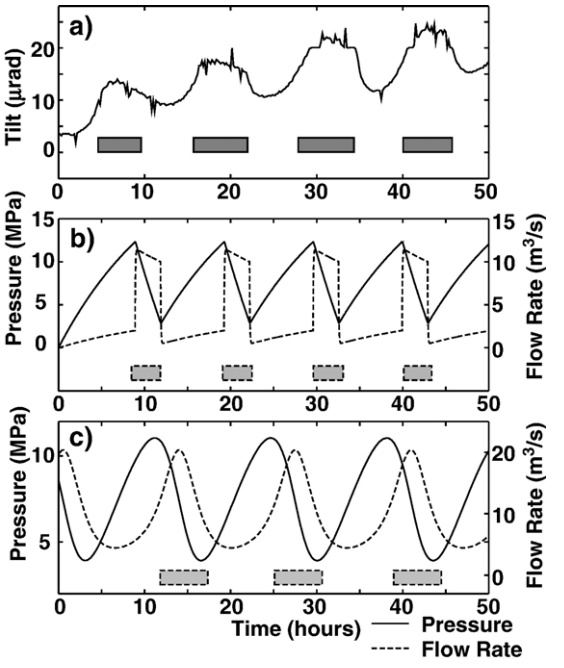

Fig. 12. A comparison of (a) the data and the models of (b) Denlinger and Hoblitt (1999) and (c) Wylie et al. (1999). In panel (a), the tilt is given as the solid line and the occurrence of low-frequency seismic family swarms is represented by the oblongs. The start of the oblong represents the first event of the swarm and the end represents the last event. In (b) and (c), the solid line represents the pressure and the dashed line represents the flow rate. The oblongs in these two panels represent the times at which seismicity is expected to occur.

4.2. The swarm structure

Deformation and seismicity are well correlated (Fig. 12a), with the results showing that the onset of low-frequency earthquake families tends to precede the change from accelerating to decelerating inflation. This suggests that the seismicity indicates the initiation of a depressurisation process. The cessation of the waveform families, coincident with the change from accelerating to decelerating deflation, suggests that the seismicity stops when this depressurisation process becomes inactive or has negligible effect. The regular temporal pattern of family initiation within the swarms (Fig. 8) indicates that the sequence of processes causing the seismicity are repeated from swarm to swarm.

Several mechanisms have been proposed for the cyclic behaviour observed at silicic volcanoes, including Soufrière Hills. These attempt to reproduce the deformation signals, but not the occurrence of seismicity. We discuss below two models, which seek to explain the observed periodic behaviour, including the tilt cycles. We assess where seismicity is most likely to occur in these models and compare with our observations.

Denlinger and Hoblitt (1999) model a compressible magma within a cylindrical conduit undergoing Newtonian flow due to magma being supplied at a constant rate from below. Once a given threshold flow rate is exceeded a stick-slip condition is invoked allowing magma to slip along a shallow portion of the conduit wall, reducing the pressure within the system (Fig. 12b). The most obvious trigger for seismicity in this model is the activation of the shear zone, by brittle failure, along which a magma plug can slip.

The possibility for brittle fracture of magma is widely reported (Dingwell, 1996; Tuffen et al., 2003) and has been suggested as a trigger mechanism for low-frequency earthquakes at both Unzen Volcano, Japan (Goto, 1999) and Soufrière Hills (Neuberg et al., 2006-this issue). Further evidence for such processes are the prominent vertical striations observed on extruded spines, which are thought to originate along faults or shear zones within the conduit (Sparks et al., 2000).

The onset of seismicity in the Denlinger and Hoblitt (1999) model would therefore occur at the time when slip is initiated at the conduit wall. This coincides with the maximum pressure in their model, assumed to be

associated with the peak of the tilt cycle (Fig. 12b). This is incompatible with our observations, as is the implication that the seismicity would stop when the tilt was at a minimum.

The model of Wylie et al. (1999) includes no mechanism which produces rapid jumps in flow rate, such as the stick-slip motion invoked by Denlinger and Hoblitt (1999). Rather, the model is comprised of a two section conduit; a lower conduit, where the magma is assumed to be gas-charged, undergoing no exsolution and of a constant viscosity, and an upper conduit where exsolution is initiated, causing the viscosity of the melt to increase. The flow rate into the base of the lower conduit is fixed and pressure builds up underneath the degassed, highly viscous, upper conduit. This pressurisation slowly increases the flow rate of the low viscosity, gas-charged, magma into the upper conduit. The lower viscous resistance of the rising magma allows an increased flow rate into the upper conduit, reducing the time available for exsolution of volatiles and therefore the viscosity remains low. This rapid increase in magma motion decreases the pressure in the lower conduit, which eventually causes a decrease in flow rate. At lower flow rates, the magma in the upper conduit has more time to exsolve gases and therefore becomes highly viscous again. These processes repeat, cycling the pressure and flow rate conditions (Fig. 12c).

There is no explicit stick-slip mechanism within this model, yet the rapid increase in flow rate through the upper conduit suggests the highly viscous magma moves as a plug. The increase in flow rate occurs close to the inflection point in the pressure–time graph (Fig. 12c), when depressurisation due to increased flow rates begins to have a greater effect. Such a flow is expected to produce areas of increased shear and high strain rates at the conduit wall thus allowing brittle failure to occur. The timing of this failure closely fits the seismic observations. However, if the seismicity is associated with high flow rates, at the end of the swarm the earthquakes would stop at approximately the time when pressure falls to a minimum, which is not consistent with the results (Fig. 12a).

Both the models of Denlinger and Hoblitt (1999) and Wylie et al. (1999) produce pressure fluctuations, which approximate the deformation observed at Soufrière Hills yet neither satisfactorily reproduce the seismicity patterns. Voight et al. (1999) suggested that hydrofracturing leading to the escape of pressurised gases, and a subsequent depressurisation of the system, would occur as the conduit gas pressure increased towards the critical level required for extrusion or explosion. The fracturing model of Neuberg et al. (2006-this issue) is also appropriate, assuming that high pressures lead to increased flow rates and therefore high strain rates. Evidence for such gas movement has been inferred from tuffisite veining observed in fossil conduits (Stasiuk et al., 1996; Tuffen and Dingwell, 2005). Fracturing, causing gas loss, would produce the correct pattern of seismicity; as the pressure increases, it reaches a level at which fracturing occurs releasing gas; this acts to depressurise the system causing the tilt to pass through an inflection point. As the pressure continues to rise, due to the pressurisation still being dominant over the depressurisation, the rate of seismicity would increase as the fractures become more active in order to release the excess pressure. Eventually, the gas loss would become dominant and the tilt would record a deflation. This result agrees qualitatively with the SO_2 emission results of Watson et al. (2000), which show that gas loss is greatest in the deflation stage of tilt cycles. As the pressure decreases further, the flow rate would drop, strain rates would decrease, new fractures would not be formed and the low-frequency seismicity would cease. The further deflation may be due to degassing along the brecciated conduit margins (Rust et al., 2004) or pre-existing fractures before these become filled with ash, closing the system and allowing the conduit to pressurise again.

The proposed gas release mechanism can also account for the finite numbers of waveform families, if it is assumed that only a finite number of fractures undergo brittle failure as observed in preserved rhyolitic conduits (Tuffen et al., 2003). The repeated brittle failure of one fracture acts as the trigger for one waveform family. The location of this brittle failure can remain constant, even in flowing magma, as the actively fracturing section is always located at the position where the magma passes from the ductile to brittle flow regime, as described by Neuberg et al. (2006-this issue).

4.3. Effect of the dome collapse

Although the dome collapse caused activity at some source locations to pause for 28 h, it did not destroy the sources. Therefore, this low-frequency seismicity cannot be produced in shear zones and fractures within the dome as suggested by Sparks et al. (2000). Again, the waveforms did not evolve significantly so the removal of an overburden equivalent to 3 MPa disrupts the activity pattern but does not modify the origin of the seismic waves. The rise in activity of some groups and the reduction in others suggests a change in the equi-

librium of the system as would be expected after a decompression. If, for example, the seismicity was caused by repeated fracture along shear zones within the magma (Tuffen et al., 2003), this shift in dominant source locations may indicate a shift in the position of the critical region in which brittle failure can occur (Neuberg et al., 2006-this issue). The reactivation of the 'A' families a day after the event may be related to the emergence of a shear lobe following the collapse, first observed on the 27th June (Watts et al., 2002). We speculate that at this time the rising magma has, through the processes of volatile diffusion and exsolution, attained similar pressure and viscosity conditions at the critical region for brittle failure to those existing before the collapse.

5. Conclusions

Waveforms at the Soufrière Hills Volcano in Montserrat can be classified into groups on the basis of their similar waveforms. The methodology presented in this paper provides a simple and efficient method for systematically classifying events into groups that have significant physical meaning. Each group represents a set of events that have been triggered within a small source volume leading to conduit resonance. The resulting wave-field is then radiated along an identical path to the receiver.

For the 6 days of analysis presented here, it is shown that a discrete set of seismic sources act regularly and repeatedly within the upper conduit system. These groups form two subsets. The first have a high degree of similarity with each other; the differences are highlighted by the variation in the relative amplitudes of excited frequencies. The second subset contains waveforms, which are independent of all others. This suggests that there may be one resonating body, e.g. a conduit section, which is the most active and a series of other resonators that have low levels of persistent activity.

The sources are extremely stable and do not significantly evolve through a period of high-amplitude shallow deformation and a major dome collapse. This places constraints on the location and mechanism for low-frequency seismicity. In particular, the repeatability of the patterns of waveform groups between swarms indicates that the mechanism for shallow pressurisation is extremely well ordered with different seismic sources being reactivated in the same manner for each deformation cycle.

We have compared our observations with proposed models for cyclic behaviour at silicic volcanoes and find that the proposed mechanisms do not account for the temporal seismicity pattern. A qualitative model based on gas release through brittle fractures appears to agree with the time at which seismicity occurs and the presence of distinct waveform families. Future quantitative models of cyclic behaviour should consider both temporal and spatial patterns of deformation and seismicity in order to better constrain the physical processes that drive the system.

Acknowledgements

This work was funded by NERC through PhD grant NER/S/A/2002/10478 and by MULTIMO (Contract No. EVG1-CT-2000-00021), which is supported by the Environmental and Sustainable Development Program of the European Commission Research Directorate General. The data collection and archiving by staff of the Montserrat Volcano Observatory is fully acknowledged. We thank S. Sturton for original suggestions, and L. Collier, A. Jolly and H. Tuffen for useful discussions. Constructive reviews by P. Lesage, T. Ohminato and O. Navon greatly improved this manuscript.

References

Barclay, J., Rutherford, M., Carroll, M., Murphy, M.D., Devine, J.D., Gardner, J., Sparks, R.S.J., 1998. Experimental phase equilibria constraints on pre-eruptive storage conditions of the Soufrière Hills magma. Geophys. Res. Lett. 25 (18), 3437–3440.

Chouet, B., 1988. Resonance of a fluid-driven crack: radiation properties and implications for the source of long-period events and harmonic tremor. J. Geophys. Res. 93 (B5), 4375–4400.

Denlinger, R.P., Hoblitt, R.P., 1999. Cyclic eruptive behavior of silicic volcanoes. Geology 27 (5), 459–462.

Dingwell, D., 1996. Volcanic dilemma: flow or blow? Science 273, 1054–1055.

Fremont, M.-J., Malone, S.D., 1987. High precision relative locations of earthquakes at Mount St. Helens, Washington. J. Geophys. Res. 92 (B10), 10223–10236.

Geller, R.J., Mueller, C.S., 1980. Four similar earthquakes in central California. Geophys. Res. Lett. 7 (10), 821–824.

Gil Cruz, F., Chouet, B.A., 1997. Long-period events, the most characteristic seismicity accompanying the emplacement and extrusion of a lava dome in Galeras Volcano, Columbia, in 1991. J. Volcanol. Geotherm. Res. 77 (1–4), 121–158.

Goto, A., 1999. A new model for volcanic earthquakes at Unzen Volcano: melt rupture model. Geophys. Res. Lett. 26 (16), 2541–2544.

Miller, A., Stewart, R.L., White, R.A., Luckett, R., Baptie, B.J., Aspinall, W.P., Latchman, J.L., Lynch, L., Voight, B., 1998. Seismicity associated with dome growth and collapse at the Soufrière Hills Volcano, Montserrat. Geophys. Res. Lett. 25 (18), 3401–3404.

Neuberg, J., 2000. Characteristics and causes of shallow seismicity in andesite volcanoes. Philos. Trans. R. Soc. Lond., A 358, 1533–1546.

Neuberg, J., Luckett, R., Baptie, B., Olsen, K., 2000. Models of tremor and low-frequency earthquake swarms on Montserrat. J. Volcanol. Geotherm. Res. 101 (1–2), 83–104.

Neuberg, J., Tuffen, H., Collier, L., Green, D.N., Powell, T., Dingwell, D.B., 2006. The trigger mechanism of low-frequency earthquakes on Montserrat. J. Volcanol. Geotherm. Res. 153, 37–50. doi:10.1016/j.jvolgeores.2005.08.008.

Power, J.P., Lahr, J.C., Page, R.A., Chouet, B.A., Stephens, D.H., Harlow, T.L., Murray, T.L., Davies, J.N., 1994. Seismic evolution of the 1989–1990 eruption sequence of Redoubt Volcano, Alaska. J. Volcanol. Geotherm. Res. 62 (1–4), 69–94.

Rowe, C.A., Thurber, C.H., White, R.A., 2004. Dome growth behaviour at Soufrière Hills Volcano, Montserrat, revealed by relocation of volcanic event swarms, 1995–1996. J. Volcanol. Geotherm. Res. 134 (3), 199–221.

Rust, A.C., Cashman, K.V., Wallace, P.J., 2004. Magma degassing buffered by vapor flow through brecciated conduit margins. Geology 32 (4), 349–352.

Sparks, R.S.J., Murphy, M.D., Lejeune, A.M., Watts, R.B., Barclay, J., Young, S.R., 2000. Control on the emplacement of the andesite lava dome of the Soufrière Hills Volcano, Montserrat by degassing-induced crystallisation. Terra Nova 12, 14–20.

Stasiuk, M.V., Barclay, J., Carroll, M.R., Jaupart, C., Ratte, J.C., Sparks, R.S.J., Tait, S.R., 1996. Degassing during magma ascent in the Mule Creek vent (USA). Bull. Volcanol. 58 (2–3), 117–130.

Stephens, C.D., Chouet, B.A., 2001. Evolution of the December 14, 1989 precursory long-period event swarm at Redoubt Volcano, Alaska. J. Volcanol. Geotherm. Res. 109 (1–3), 133–148.

Sturton, S., Neuberg, J., 2003. The effects of a decompression on seismic parameter profiles in a gas-charged magma. J. Volcanol. Geotherm. Res. 128 (1–3), 187–199.

Tuffen, H., Dingwell, D., 2005. Fault textures in volcanic conduits: evidence for seismic trigger mechanisms during silicic eruptions. Bull. Volcanol. 67, 370–387.

Tuffen, H., Dingwell, D.B., Pinkerton, H., 2003. Repeated fracture and healing of silicic magma generates flow banding and earthquakes? Geology 31 (12), 1089–1092.

Umakoshi, K., Shimizu, H., Matsuwo, N., 2002. Seismic activity associated with the growth of the lava dome at Unzen Volcano (November 1993–January 1994)—grouping of earthquakes on the basis of cross-correlations among their waveforms. Bull. Volcanol. Soc. Jpn. 47, 43–55 (in Japanese, Abstract in English).

Umakoshi, K., Shimizu, H., Matsuwo, N., 2003. Seismic activity associated with the endogenous growth of lava dome at Unzen Volcano, Japan. Abstract V10/01A/D-014, IUGG XXIII Meeting, Sapporo, Japan.

Voight, B., Hoblitt, R.P., Clarke, A.B., Lockhart, A.B., Miller, A.D., Lynch, L., McMahon, J., 1998. Remarkable cyclic ground deformation monitored in real-time on Montserrat, and its use in eruption forecasting. Geophys. Res. Lett. 25 (18), 3405–3408.

Voight, B., Sparks, R.S.J., Miller, A.D., Stewart, R.C., Hoblitt, R.P., Clarke, A., Ewart, J., Aspinall, W.P., Baptie, B., Calder, E.S., Cole, P., Druitt, T.H., Hatford, C., Herd, R.A., Jackson, P., Lejeune, A.M., Lockhart, A.B., Loughlin, S.C., Luckett, R., Lynch, L., Norton, G.E., Robertson, R., Watson, I.M., Watts, R., Young, S.R., 1999. Magma flow instability and cyclic activity at Soufrière Hills Volcano, Montserrat, British West Indies. Science 283, 1138–1142.

Watson, I.M., Oppenheimer, C., Voight, B., Francis, P.W., Clarke, A., Stix, J., Miller, A., Pyle, D.M., Burton, M.R., Young, S.R., Norton, G., Loughlin, S., Darroux, B., MVO Staff, 2000. The relationship between degassing and ground deformation at Soufrière Hills Volcano, Montserrat. J. Volcanol. Geotherm. Res. 98 (1–4), 117–126.

Watts, R.B., Herd, R.A., Sparks, R.S.J., Young, S.R., 2002. Growth patterns and emplacement of the andesitic lava dome at Soufrière Hills Volcano, Montserrat. In: Druitt, T.H., Kokelaar, B.P. (Eds.), The Eruption of Soufrière Hills Volcano, Montserrat, From 1995 to 1999. Geological Society Memoirs, London, vol. 21, pp. 115–152.

White, R.A., Miller, A.D., Lynch, L., Power, J., 1998. Observations of hybrid seismic events at Soufrière Hills Volcano, Montserrat: July 1995 to September 1996. Geophys. Res. Lett. 25 (19), 3657–3660.

Wylie, J.J., Voight, B., Whitehead, J.A., 1999. Instability of magma flow from volatile-dependent viscosity. Science 285, 1883–1885.